Effects of the 5 Alpha-Reductase Inhibitor Dutasteride on Gene Expression in Prostate Cancer Xenografts

Lucy J. Schmidt,[1] Kevin M. Regan,[1] S. Keith Anderson,[2] Zhifu Sun,[2] Karla V. Ballman,[2] and Donald J. Tindall[1,3]*

[1]*Department of Urology Research, Mayo Clinic College of Medicine, Mayo Clinic, Rochester, Minnesota*
[2]*Division of Biomedical Statistics and Informatics, Mayo Clinic College of Medicine, Mayo Clinic, Rochester, Minnesota*
[3]*Department of Biochemistry and Molecular Biology, Mayo Clinic College of Medicine, Mayo Clinic, Rochester, Minnesota*

BACKGROUND. In the prostate, androgens play a crucial role in normal and cancerous growth; hence the androgenic pathway has become a target of therapeutic intervention. Dutasteride is a 5 alpha-reductase (5AR) inhibitor currently being evaluated both for chemoprevention and treatment of prostate cancer. Dutasteride inhibits both 5AR I and II enzymes, effectively blocking conversion of testosterone to dihydrotestosterone (DHT) in the prostate. This greatly reduces the amount of the active ligand DHT available for binding to the androgen receptor (AR) and stimulating proliferation, making this a good candidate for chemoprevention of prostate cancer. In this study, we sought to determine how dutasteride is functioning at the molecular level, using a prostate cancer xenograft model.
METHODS. Androgen-responsive LuCaP 35 xenograft tumors were grown in Balb/c mice. Subcutaneously implanted time-release pellets were used for drug delivery. Microarray analysis was performed using the Affymetrix HG-U133Av2 platform to examine changes in gene expression in tumors following dutasteride treatment.
RESULTS. Dutasteride significantly reduced tumor growth in LuCaP 35 xenografts by affecting genes involved in apoptotic, cytoskeletal remodeling, and cell cycle pathways among others. Notably, genes in the Rho GTPase signaling pathway, shown to be important in androgen-deprivation conditions, were significantly up-regulated.
CONCLUSION. We have identified multiple pathways outside of the androgenic pathway in prostate cancer xenografts affected by treatment with dutasteride. These findings provide insights into the function of dutasteride within the tumor microenvironment, potentially allowing for development of agents that can be used in combination with this drug to further enhance its effectiveness. *Prostate 69: 1730–1743, 2009.*

KEY WORDS: **dutasteride; prostate; xenograft**

INTRODUCTION

Prostate cancer continues to be a leading cause of cancer death in males worldwide. In the prostate, androgens play a crucial role in both normal and cancerous growth; hence, the androgenic pathway has become a target of therapeutic intervention. Testosterone is converted by 5 alpha-reductase (5AR) isoenzymes to the more potent ligand dihydrotestosterone (DHT), which binds to the androgen receptor

Additional Supporting Information may be found in the online version of this article.

Donald J. Tindall is a consultant for GlaxoSmithKline.

Grant sponsor: NCI; Grant numbers: CA121277, CA125747, CA91956; Grant sponsor: T.J. Martell Foundation; Grant sponsor: GlaxoSmithKline; Grant number: 144.

*Correspondence to: Donald J. Tindall, Department of Urology Research, Mayo Clinic College of Medicine, 200 First Street SW, Rochester, MN 55905. E-mail: tindall.donald@mayo.edu
Received 24 April 2009; Accepted 1 July 2009
DOI 10.1002/pros.21022
Published online 12 August 2009 in Wiley InterScience (www.interscience.wiley.com).

(AR) thus promoting proliferation and survival of target tissues, such as the prostate. Dutasteride is a novel dual 5AR inhibitor (SRD5I) that is currently being investigated as a potential chemopreventive agent for prostate cancer in the REduction by DUtasteride of prostate Cancer Events (REDUCE) trial [1]. By blocking the conversion of testosterone to DHT, dutasteride reduces the amount of the more active ligand, resulting in reduced proliferative activity of the cells within the prostate. The REDUCE trial is designed to determine if dutasteride administered at 0.5 mg daily decreases the risk of biopsy detectable prostate cancer. Another clinical trial, the Reduction by Dutasteride of Clinical Progression Events in Expectant Management (REDEEM), is evaluating whether dutasteride extends time to prostate cancer progression [2]. These trials underscore the need for a better understanding of how dutasteride is working at the molecular level.

Dutasteride has been shown to kill prostate cancer cells both in vitro [3,4] and in vivo [5,6]. In previous studies we determined changes in gene expression profiles in a number of prostate cancer cell lines following dutasteride treatment in vitro [4,7]. In the current study we have extended these findings to a mouse model, using microarray analysis of prostate cancer xenografts, in order to delineate effects of the tumor-host microenvironment.

MATERIALS AND METHODS

LuCaP Xenografts and Drug Treatment

The LuCaP 35 androgen-dependent prostate cancer xenograft was obtained from Dr. Robert Vessella (University of WA, Seattle) and was maintained by passage in athymic Balb/c mice (Harlan Labs, Indianapolis, IN). Animals were housed in the Mayo Clinic pathogen-free rodent facility, and all procedures performed were approved by the Mayo Clinic Institutional Animal Care and Use Committee. For this study, newly inoculated tumors were allowed to proliferate for 6 weeks, at which time dutasteride or placebo pellets formulated by Innovative Research (Innovative Research of America, Sarasota, FL) were implanted subcutaneously. The dutasteride pellets were time-release pellets designed to deliver 1 mg/kg/day of drug. Mice were bled pre-implantation for baseline serum values of both PSA and testosterone and initial tumor measurements noted. After 8 days of treatment, mice were bled, sacrificed, and tumors harvested into liquid nitrogen. Tumor tissue was stored at -80°C.

Serum Testing

Serum samples were obtained by cheek bleeds of mice using Microtainer tubes (BD, San Jose, CA). Serum testosterone levels were measured by coated well ELISA (DSL, Webster, TX) both before and after pellet implantation to verify drug delivery. Serum PSA levels were determined by ELISA (DSL) pre- and post-implantation. All samples were run in duplicate.

RNA Preparation and Microarray

RNA was isolated from xenograft tumor tissue using Trizol (Invitrogen, Carlsbad, CA) followed by purification on RNeasy columns (Qiagen, Germantown, MD) then checked for integrity by Agilent testing (Affymetrix, Santa Clara, CA). Subsequently, cDNA was generated and hybridized to Affymetrix HG-U133Av2 DNA microarrays following manufacturer's protocol in the Mayo Advanced Genomics Technology Microarray Shared Resource core facility.

Statistical Analysis

Microarray results were analyzed using the software R and R-packages *fastlo* and *rma*. The non-background corrected intensity data from the Affymetrix CEL files were normalized using *fastlo* [8] a faster model-based intensity-dependent normalization method that produces results essentially the same as those from cyclic loess [9]. Subsequently, the probe-level data for each probeset was summarized using Tukey's median polish [10] implemented in the *rma* package. The summarized probeset values represent an overall measure of expression for the corresponding gene. To assess differential expression between the dutasteride and placebo groups the statistical *t*-test assuming unequal variances was utilized. A false discovery rate [11], which is the expected proportion of false discoveries amongst the rejected hypotheses, was calculated for each probeset. A fold-change ratio was calculated for each probeset based on the average expression for the placebo group divided by the average expression for the dutasteride group. Probesets that were deemed significant were then sorted by the log 2-transform of this fold-change ratio. Pathway analysis was performed using MetaCore pathway analysis and data mining application GeneGo. The differentially expressed genes with P-values ≤ 0.05 (2,062 probesets) selected from the previous step were used as focus genes and the Affymetrix HG-U133Av2 gene list used as reference.

Real-Time PCR

Two-step real-time PCR was performed using cDNA prepared from RNA described above using SuperScript III First-Strand Synthesis System for RT-PCR (Invitrogen) and SYBR Green PCR Master Mix (Applied Biosystems, Foster City, CA) on an ABI

PRISM 7700 SDS following manufacturer's instructions. Primers for SYBR green amplification were designed using the Primer3 software (http://www-genome.wi.mit.edu/cgi-bin/primer/primer3_www.cgi) and both forward and reverse primers were used at a final concentration of 900 nM. PCR products (120–150 bp) were run on 1.2% agarose gels to check for non-specific amplification. Relative expression levels were determined by the comparative C_T method using the formula $2^{-\Delta\Delta C_T}$ where C_T is the threshold cycle of amplification. Samples were run in triplicate with primers to GAPDH used for normalization.

RESULTS

Xenograft Response to Dutasteride Treatment

LuCaP 35 androgen-dependent prostate xenograft tumors were developed along with their androgen-independent variant LuCaP 35V as a model for studying progression to androgen independence. The LuCaP 35 tumors express a wild-type AR, produce PSA and respond to androgen ablation comparable to that observed in humans [12], making this an ideal model for studying drug response. Dutasteride was delivered using time-release pellets and parameters of drug delivery were initially determined by implanting the pellets and monitoring serum testosterone levels in the mice. The dutasteride time-release pellets were designed to deliver 1 mg/kg/day of drug. As dutasteride inhibits the conversion of testosterone to DHT, the resultant elevated serum levels of testosterone were used as an indicator of successful drug delivery. We performed several trials using this method to monitor drug delivery and found that by 7–10 days serum testosterone levels were consistently elevated (data not shown). Our objective was to examine early molecular events occurring with dutasteride treatment, so we limited treatment time to that which would achieve adequate drug exposure without compromising the ability to detect early gene response. We know from previous work with PCa cells in vitro that significant changes in gene expression are occurring at this time with dutasteride treatment [4,7].

Fig. 1. Time-release pellets (Innovative Research) were implanted subcutaneously in the posterior dorsal flank of tumor-bearing Balb/c mice. Pellets were formulated to deliver placebo or 1 mg/kg/day dutasteride.

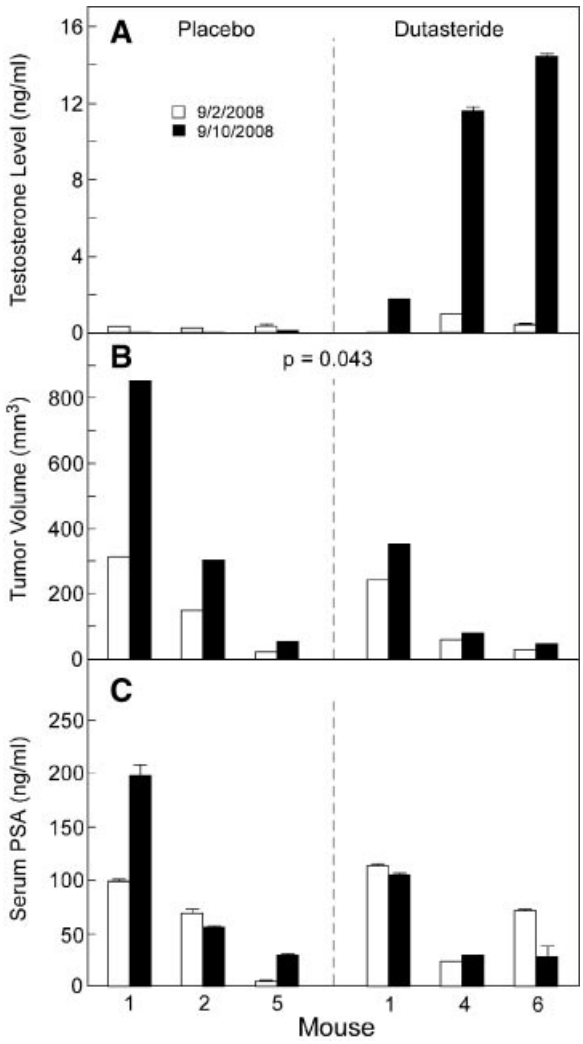

Fig. 2. **A**: Serum testosterone levels of mice bearing LuCaP 35 xenografts were determined by EIA pre- and post-treatment. The graphed values represent the six mice chosen for the microarray analysis. Measurements were performed on duplicate serum samples. **B**: Tumor volumes were measured before and after treatment. Tumor growth in the dutasteride group was significantly less than in the placebo group, $P = 0.0426$. **C**: Serum PSA levels of the xenograft-bearing mice were determined by EIA pre- and post-treatment. There is no statistically significant difference in the change in PSA values between placebo- and dutasteride-treated mice, $P = 0.3031$.

TABLE I. Gene Expression Changes With Dutasteride Treatment

Gene symbol	GenBank ID	*P*-value	Absolute value FC rank	Fold-change log 2 difference[a]	Fold-change ratio
GAGE7	NM_021123	0.04474	2	1.02788	2.03903
GAGE4	NM_001474	0.01777	9	0.84794	1.79994
CRISP3	NM_006061	0.02990	12	0.77208	1.70773
GAGE2A	NM_001472	0.02427	15	0.75012	1.68193
GAGE3	NM_001473	0.03036	17	0.73002	1.65866
VEGFA	M27281	0.02072	23	−0.70670	0.61271
VEGFA	H95344	0.02426	25	−0.67068	0.62820
TNFSF10	NM_003810	0.02108	26	−0.65943	0.63312
PRKAR2B	NM_002736	0.00011	37	0.59993	1.51564
VEGFA	AF091352	0.04010	43	−0.59132	0.66373
WNT5A	NM_003392	0.00387	48	0.58433	1.49935
NA	AI683552	0.03100	49	−0.58335	0.66740
UGT1A3	NM_019093	0.04432	50	−0.58285	0.66764
VEGFA	AF022375	0.00332	53	−0.57502	0.67127
TNFSF10	NM_003810	0.03174	54	−0.57448	0.67152
ID1	D13889	0.01604	57	−0.55902	0.67876
HDGF2	NM_017932	0.01897	61	−0.55487	0.68071
KRT19	NM_002276	0.00853	63	−0.55315	0.68152
SGCE	NM_003919	0.01548	67	0.54656	1.46060
ELOVL2	NM_017770	0.04760	69	0.53877	1.45273
MAGl1	AW971248	0.00900	71	−0.53347	0.69088
KLC1	AF222691	0.02334	73	−0.52737	0.69381
FKBP5	NM_004117	0.01774	79	0.52055	1.43450
NA	AL050204	0.01408	81	−0.51211	0.70119
CCNE2	AF112857	0.04400	84	0.50782	1.42190
CKB	NM_001823	0.03943	89	−0.49911	0.70754
MAFF	NM_012323	0.01385	90	−0.49412	0.70999
IER3	NM_003897	0.01244	95	−0.48566	0.71416
APOD	NM_001647	0.03787	100	0.48025	1.39499
PEG10	BE858180	0.00600	106	0.47058	1.38567
E2F8	NM_024680	0.04821	109	0.46956	1.38468
NA	BC002629	0.00957	116	−0.46387	0.72503
NA	N35922	0.01005	118	−0.46047	0.72674
IL32	NM_004221	0.01119	121	−0.45818	0.72790
SKP2	BC001441	0.00936	123	0.45757	1.37323
UGT1A6	NM_001072	0.03577	124	−0.45602	0.72899
ZNF611	NM_030972	0.01253	126	−0.45529	0.72935
DNASE1L3	NM_004944	0.02874	128	0.45459	1.37039
USP34	NM_014709	0.02646	130	−0.45362	0.73020
GAL	AL556409	0.01603	133	0.45153	1.36749
LOC152719	AK021514	0.03628	135	−0.44954	0.73227
PLAU	NM_002658	0.01385	136	−0.44705	0.73353
MAT2A	BC001686	0.04503	140	0.43779	1.35453
RFC3	BC000149	0.01923	141	0.43771	1.35445
NA	NM_025120	0.01397	144	−0.43541	0.73948
MAGI1	AU146794	0.03671	146	−0.43454	0.73992
C11orf71	NM_019021	0.04871	148	0.43309	1.35012
TMPO	AF113682	0.01581	150	0.43102	1.34819
ELOVL2	BF508639	0.03353	154	0.42948	1.34675
CECR7	NM_021031	0.01906	157	−0.42679	0.74391
MAFB	NM_005461	0.04744	159	0.42215	1.33992
ANKRD10	AF131777	0.03342	160	−0.42059	0.74711
CCNE2	NM_004702	0.02001	161	0.41847	1.33651

TABLE I. (*Continued*)

Gene symbol	GenBank ID	*P*-value	Absolute value FC rank	Fold-change log 2 difference[a]	Fold-change ratio
FHL2	NM_001450	0.01185	162	−0.41770	0.74861
LOC728686	NM_024796	0.01550	165	0.41559	1.33385
RAB31	AF183421	0.04856	167	−0.41424	0.75041
EXPH5	AB014524	0.02086	171	−0.41104	0.75208
SPG21	AL137312	0.02853	174	−0.40907	0.75310
NA	NM_013344	0.03606	179	−0.40786	0.75373
NXT2	AK023289	0.03688	181	0.40776	1.32662
HIST1H4C	NM_003542	0.04069	182	0.40623	1.32522
RFC5	NM_007370	0.01275	184	0.40539	1.32444
DHFR	NM_000791	0.00118	185	0.40493	1.32402
RNASEH2A	NM_006397	0.03241	186	0.40488	1.32398
ARL6IP2	AW301806	0.03658	188	−0.40318	0.75618
LOC389517	AK024602	0.01966	191	−0.40111	0.75727
PODNL1	NM_024825	0.02883	192	−0.40069	0.75749
JUN	BE327172	0.03828	198	−0.39805	0.75887
ALMS1	AB002326	0.02867	199	−0.39677	0.75955
TAF9B	AF077053	0.01320	200	0.39575	1.31563

[a]Positive values indicate placebo expression was higher.
Affymetrix HG-U133Av2 microarray: Genes significantly affected by dutasteride treatment of LuCaP 35 xenografts ranked by absolute value of log 2 fold-change. The entire list can be viewed at http://www3.interscience.wiley.com.

For this study, LuCaP 35 tumor tissue was inoculated into athymic Balb/c mice and allowed to proliferate for 6 weeks. Tumor growth rates and volumes varied so at the time of treatment mice were randomly sorted into pairs with similarly matched tumor sizes. Mice were bled pre-implantation for baseline serum values of both PSA and testosterone and initial tumor volumes were measured. Pellets were then implanted subcutaneously in the posterior dorsal flank, as pictured in Figure 1, with half of the mice receiving placebo pellets and the other half receiving dutasteride pellets. After 8 days of treatment, mice were bled and sacrificed, and tumors were harvested and measured. At that time, mice from each group that demonstrated the best response to the dutasteride treatment, as determined by serum testosterone levels, were chosen for RNA isolation and further analysis. Figure 2A shows the testosterone levels of the mice chosen for microarray analysis.

The rate of tumor growth was diminished significantly in the dutasteride-treated mice when compared to the placebo group (Fig. 2B, dutasteride mice average increase $46 \pm 9\%$ vs. placebo average increase $133 \pm 35\%$, P-value $= 0.04263$). Although PSA levels for the most part paralleled tumor volume, no statistically significant effect of dutasteride treatment on PSA levels was found, $P = 0.3031$ (Fig. 2C). This is not unexpected; it is important to note that treatment with an SRD5I like dutasteride is not the same as castration or androgen ablation and although DHT levels have been diminished, the increased testosterone levels can also continue to regulate tumor growth and androgen-regulated genes such as PSA. While tumor size and PSA levels are not decreased dramatically at this time point, testosterone levels are elevated, indicating effective drug uptake, so this appears to be a relevant time point for measuring early gene expression changes with respect to dutasteride treatment that may eventually affect tumor response.

Gene Expression Changes With Dutasteride Treatment

RNA samples obtained from xenograft tumors of the three placebo- and three dutasteride-treated mice shown in Figure 2A were used to generate cDNA probes, which were hybridized to Affymetrix HG-U133Av2 microarrays. Table I is a partial list of the array data ranked by absolute value of log 2 fold-change. The entire list can be viewed at http://www3.interscience.wiley.com. The top 100 genes affected by dutasteride treatment are presented as a Heatmap shown in Figure 3. The top 100 were determined by selecting all probesets with an unequal-variance t-test P-value ≤ 0.05, then sorting this list of 2,062 by the absolute value of the log 2 fold-change. As with clinical cancers, LuCaP 35 tumors exhibit heterogeneous growth; after implantation,

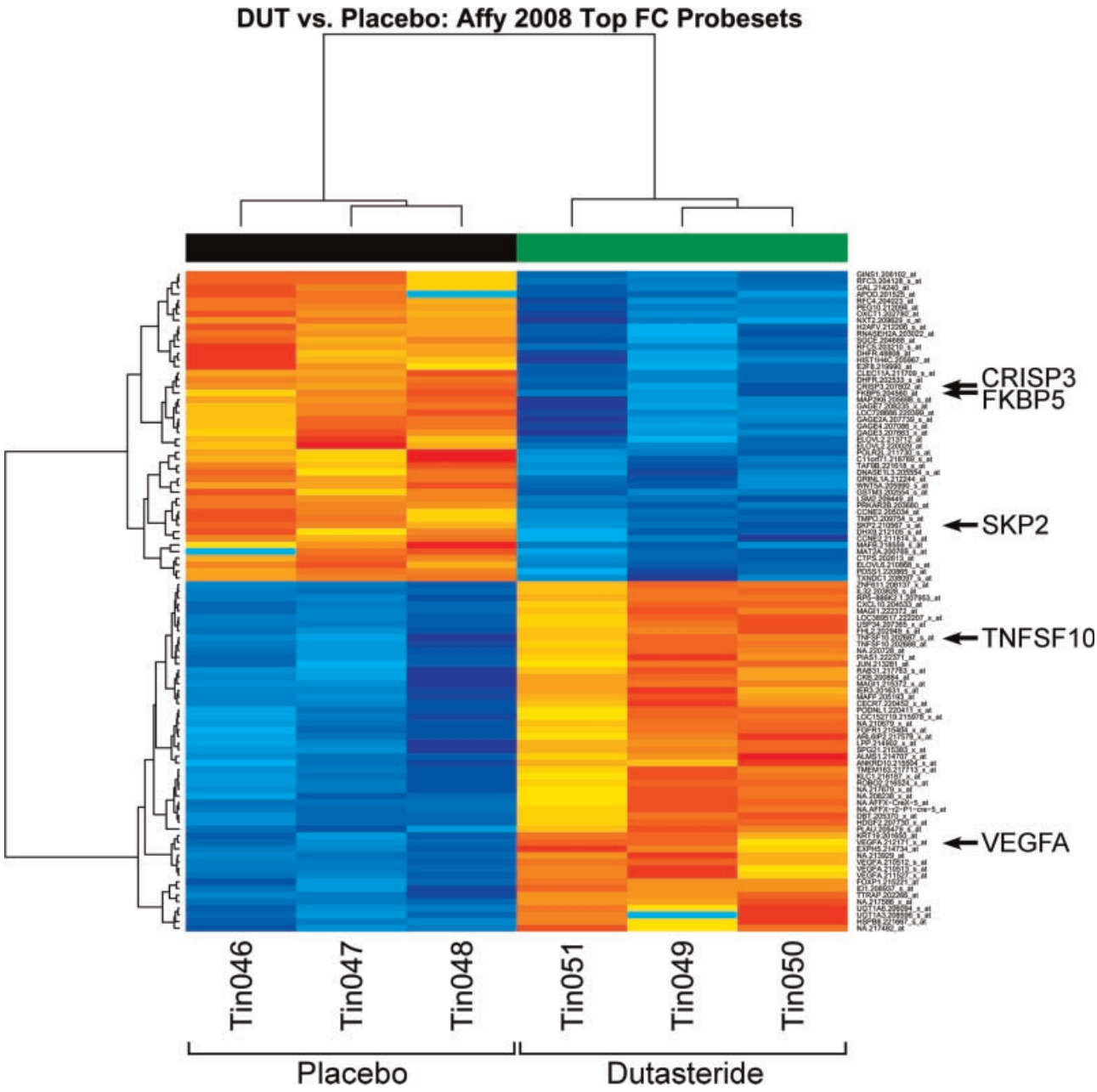

Fig. 3. Heatmap of the top 100 genes affected by dutasteride treatment of LuCaP 35 xenograft-bearing mice sorted by the absolute value of log 2 fold-change. Samples labeled Tin046-048 represent placebo-treated mice, while Tin049-051 represent those treated with dutasteride. Dark blue indicates lower expression and dark orange higher expression within each row or probeset.

tumors grew at different rates and in order to best mimic the clinical situation we included both the fast-growing and slow-growing tumors in this study. While we assayed tumors with starting volumes from <50 to >300 mm^3 in size, a number of consistent changes were observed with respect to gene expression between the tumors treated with dutasteride versus placebo (Table I and Fig. 3).

To validate the array data we used real-time PCR with primers to several genes from Table I that had significant fold-change ratios, such as *TNFSF10* (*TRAIL*) which had higher expression levels in dutasteride-treated mice and *CRISP3* which exhibited lower levels. We have demonstrated previously that genes involved in TRAIL-mediated apoptosis are induced in prostate cancer cells treated with dutasteride [4]. Moreover, there is evidence that prostate cancer patients with higher levels of *CRISP3* have a smaller probability of recurrence-free outcomes [13]. Figure 4 shows real-time profiles for five of these genes (A) and

A

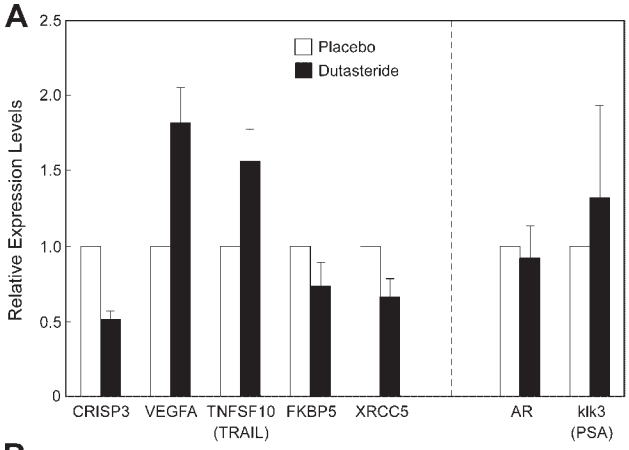

B

Affymetrix Probeset ID	Gene Symbol	GenBankID	p<0.05	p-Value	Foldchange log2 Difference	Fold-change Ratio
207802_at	CRISP3	NM_006061	yes	0.02990	0.77208	1.70773
211527_x_at	VEGFA	M27281	yes	0.02072	-0.70670	0.61271
202688_at	TNFSF10	NM_003810	yes	0.02108	-0.65943	0.63312
204560_at	FKBP5	NM_004117	yes	0.01774	0.52055	1.43450
208643_s_at	XRCC5	J04977	yes	0.00643	0.21937	1.16423
211621_at	AR	M73069	no	0.23560	0.18388	1.13594
202934_at	klk3	AI761561	no	0.45505	-0.48057	0.71669

Fig. 4. **A**: To validate microarray results real-time PCR was performed using cDNA from the LuCaP 35 xenograft tumors with gene-specific primers. Placebo value was set at 1.0 and graphed results represent average and standard deviation from three dutasteride-treated samples for each set of primers. **B**: Affymetrix HG-U133Av2 data for each of the genes examined by real-time PCR. Fold-change differences for AR and klk3 (PSA) were not significant, which was confirmed by real-time PCR, as shown in A.

corresponding Affymetrix data (B) confirming their changes in expression following treatment. Additionally, we examined the profiles of *AR* and *klk3* (*PSA*) even though these genes were not significantly affected at the mRNA level by dutasteride treatment based on the array data, and this was confirmed by real-time PCR. In our previous work with LNCaP cells in vitro, we observed a twofold increase in AR expression and a decrease in PSA [4]. This was also observed by Biancolella et al. [14] in their work examining dutasteride's effects on genes involved in androgen metabolism. Both of these studies used relatively high levels of dutasteride (10 μM), which results in marked levels of cell death. We hypothesize that with a higher drug dose or longer treatment time, our LuCaP xenografts would exhibit similar changes.

While AR mRNA levels are not consistently altered at this time point, a number of *AR* coregulators, such as *NCOA2*, *TMF1*, *PB1*, *XRCC5*, and *PIAS1* to name a few, were significantly affected (Table I and Fig. 4). It has been demonstrated that androgens can modulate AR coregulator expression, resulting in marked effects on AR activity in prostate cancer cells [15] and altered expression in these xenografts may be significant with regard to androgen regulation of genes involved in proliferation. Gene expression changes detected by array analysis were confirmed by real-time PCR for all of the genes we have chosen to examine.

Pathway Analysis

A primary goal of this study was to examine the functional pathways of the genes that were significantly affected by dutasteride treatment. The MetaCore pathways analysis tool was used to map the 2,062 probesets with *P*-values ≤ 0.05 to well-curated pathways database and functional classes. Table II lists the top 40 pathways sorted by a significant enrichment *P*-value, with 38 of these exhibiting a false discovery rate <0.25. The pathways affected by dutasteride treatment fell into categories ranging from apoptosis to lipid metabolism as illustrated in Figure 5A. The signaling pathway that was most significantly affected, cytoskeletal remodeling: regulation of actin by Rho GTPases is illustrated in Figure 5B. Of the 23 known genes in this pathway, 12 were significantly affected at the mRNA level by dutasteride treatment. This observation may be important, as it has been demonstrated previously that ligand-independent activation of the androgen receptor in prostate cancer progression can occur via Rho GTPase signaling [16], specifically in the presence of low levels of androgens. Vav3 is a Rho GTPase guanine nucleotide exchange factor (GEF) whose expression has been shown to increase in LNCaP cells with progression to androgen independence and can enhance AR activity at sub-nanomolar concentrations of androgen [17]. This gene was significantly up-regulated in the LuCaP 35 xenografts with dutasteride treatment based on our array data and was confirmed by real-time PCR (data not shown). Genes in this pathway may offer an opportunity for therapeutic intervention, whereby inhibition in addition to androgen deprivation may result in total inactivation of androgen-directed activity in prostate cancer cells.

Another potentially important observation is that the ubiquitin ligase Skp2 and related genes are down-regulated following dutasteride treatment of LuCaP 35 xenografts. Skp2 is involved in G1/S phase transition and progression through S phase in the cell cycle by degrading $p27^{Kip1}$, a negative regulator of cell cycle progression [18]. Skp2 has been found to be over-expressed in prostate cancer; elevated expression of Skp2 correlates with a poor prognosis and has been proposed as a target for therapeutic intervention [19]. Skp2, Cul1 and related cyclin-dependent kinases CDK2 and CDK4 all demonstrate decreased levels of expression in dutasteride-treated xenografts (Table I and Fig. 3), indicating this may be an additional basis for decreased proliferation in these tumors.

TABLE II. Pathways With Genes Significantly Affected by Dutasteride Treatment

	Pathway	*P*-value	Ag/Pg[a]
1	Cytoskeleton remodeling—Regulation of actin cytoskeleton by Rho GTPases	6.11E – 05	12/23
2	Transport—ACM3 in salivary glands	1.73E – 04	12/25
3	Cell cycle—Start of DNA replication in early S phase	4.88E – 04	13/31
4	Membrane-bound ESR1—Interaction with G-proteins signaling	7.45E – 04	14/36
5	Blood coagulation—GPCRs in platelet aggregation	9.25E – 04	18/53
6	Immune response—CCR3 signaling in eosinophils	1.11E – 03	19/58
7	Cell adhesion—Histamine H1 receptor signaling in interruption of cell barrier integrity	1.38E – 03	13/34
8	ATP/ITP metabolism	1.46E – 03	23/77
9	Oxidative phosphorylation	1.46E – 03	23/77
10	Inhibitory action of Lipoxin A4 on PDGF, EGF, and LTD4 signaling	1.58E – 03	10/23
11	Development—Lipoxin inhibitory action on PDGF, EGF, and LTD4 signaling	1.58E – 03	10/23
12	Development—FGFR signaling pathway	1.80E – 03	15/43
13	Muscle contraction—GPCRs in the regulation of smooth muscle tone	2.58E – 03	17/53
14	Translation—Regulation activity of EIF4F	2.79E – 03	16/49
15	Cytoskeleton remodeling—Cytoskeleton remodeling	2.94E – 03	26/95
16	Cytoskeleton remodeling—ACM3 and ACM4 in keratinocyte migration	3.07E – 03	9/21
17	Neurophysiological process—ACM regulation of nerve impulse	3.44E – 03	12/33
18	dATP/dITP metabolism	3.52E – 03	16/50
19	Development—EDG3 signaling pathway	4.67E – 03	10/26
20	DNA damage—NHEJ mechanisms of DSBs repair	5.94E – 03	8/19
21	Transcription—CREB pathway	5.96E – 03	12/35
22	Development—Endothelin-1/EDNRA transactivation of EGFR	5.96E – 03	12/35
23	Cytoskeleton remodeling—Role of PKA in cytoskeleton reorganization	6.24E – 03	11/31
24	Transcription—Transcription factor Tubby signaling pathways	6.31E – 03	6/12
25	Cell adhesion—Integrin-mediated cell adhesion and migration	6.54E – 03	14/44
26	Cardiac hypertrophy—Ca(2+)-dependent NF-AT signaling in cardiac hypertrophy	7.67E – 03	12/36
27	Immune response—Fc gamma R-mediated phagocytosis in macrophages	8.17E – 03	11/32
28	Development—MAG-dependent inhibition of neurite outgrowth	8.72E – 03	9/24
29	Immune response—CD28 signaling	1.11E – 02	13/42
30	Development—Angiotensin activation of Akt	1.17E – 02	9/25
31	Immune response—Human NKG2D signaling	1.17E – 02	9/25
32	Development—ACM3 activation of astroglial cells proliferation	1.19E – 02	8/21
33	Normal wtCFTR traffic/ER-to-Golgi	1.22E – 02	12/38
34	Development—Role of HDAC and calcium/calmodulin-dependent kinase (CaMK) in control of skeletal myogenesis	1.23E – 02	14/47
35	Cytoskeleton remodeling—TGF, WNT and cytoskeletal remodeling	1.37E – 02	26/106
36	Regulation of CFTR activity (norm and CF)	1.52E – 02	12/39
37	Oxidative stress—Role of ASK1 under oxidative stress	1.62E – 02	8/22
38	Transport—RAN regulation pathway	1.63E – 02	7/18
39	Immune response—Histamine H1 receptor signaling in immune response	1.87E – 02	12/40
40	Phospholipid metabolism p, 1	2.05E – 02	5/11

[a]Ag/Pg, array genes/pathway genes.
Pathways with genes significantly affected by dutasteride treatment of LuCaP 35 xenografts after adjusting for a false discovery rate using $P < 0.25$.

Table III shows the comparison of significantly regulated genes between the LuCaP 35 xenografts in vivo and our previous in vitro work with the androgen-responsive prostate cancer cell line LNCaP [4,7] following dutasteride treatment. The table lists the 92 Affymetrix probesets that have *P*-values of ≤ 0.05 in both the in vivo data and in vitro data that also demonstrated changes going in the same direction. By chance alone, this list would have ~28 probesets out of the 22,215 probesets, so the results well exceed that threshold lending validity to these findings. Figure 6A is a Heatmap of the 92 probesets common to both analyses, while Figure 6B shows where these common genes fit into the pathway analysis data from the LuCaP 35 xenograft data. We feel this group of common genes is especially worth examining further as they represent

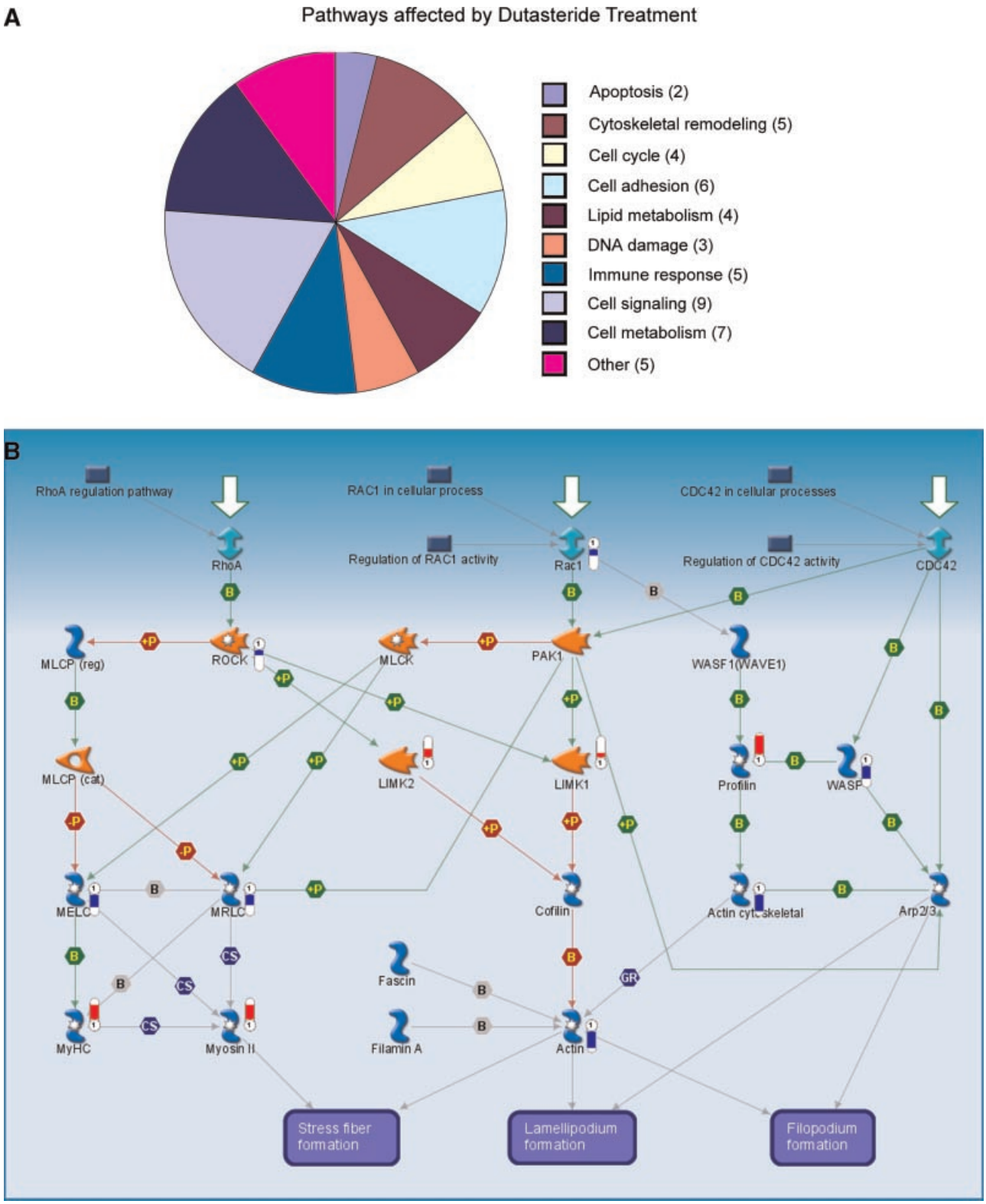

Fig. 5. **A**: Chart of pathways significantly affected by dutasteride treatment of LuCaP 35 xenografts, with the largest number of genes mapping to pathways involved in cell signaling and cell metabolism. Number of pathways is indicated in parentheses. **B**: Illustration of the top pathway affected by dutasteride treatment, with greater than half (12/23) of the known genes significantly impacted, *cytoskeletal remodeling: regulation of actin cytoskeleton by Rho GTPases*. Genes significantly affected are denoted by blue (up-regulated) or red (down-regulated) indicators.

TABLE III. Gene Expression Changes With Dutasteride Treatment In Vivo and In Vitro

			In vivo		In vitro	
Affymetrix probeset ID	Gene symbol	GenBank ID	*P*-value	Fold-change log 2 difference	*P*-value	Fold-change log 2 difference
207802_at	CRISP3	NM_006061	0.02990	0.77208	0.04738	0.24235
204560_at	FKBP5	NM_004117	0.01774	0.52055	0.02094	0.37416
211814_s_at	CCNE2	AF112857	0.04400	0.50782	0.02332	0.36431
205034_at	CCNE2	NM_004702	0.02001	0.41847	0.02966	0.33563
203210_s_at	RFC5	NM_007370	0.01275	0.40539	0.04829	0.16568
208097_s_at	TXNDC1	NM_030755	0.02798	0.38906	0.03520	0.32032
205367_at	SH2B2	NM_020979	0.02541	−0.33800	0.03765	−0.25042
201476_s_at	RRM1	AI692974	0.03132	0.33443	0.04549	0.35800
212634_at	KIAA0776	AW298092	0.01315	0.32971	0.02544	0.36242
212464_s_at	FN1	X02761	0.02578	−0.32808	0.01527	−0.52241
218025_s_at	PECI	NM_006117	0.02815	0.32105	0.03518	0.26427
215123_at	LOC23117	AL049250	0.00076	−0.30690	0.04641	−0.30002
209257_s_at	SMC3	BF795297	0.00665	0.30283	0.04114	0.32833
204119_s_at	ADK	NM_001123	0.03655	0.30198	0.01857	0.29294
210686_x_at	SLC25A16	BC001407	0.00504	−0.29824	0.03670	−0.31077
202282_at	HSD17B10	NM_004493	0.01138	0.29133	0.04802	0.18678
217299_s_at	NBN	AK001017	0.01068	0.27859	0.02646	0.34417
203427_at	ASF1A	NM_014034	0.01812	0.27375	0.02184	0.35197
206066_s_at	RAD51C	NM_002876	0.02701	0.27278	0.04248	0.25263
208120_x_at	FKSG49	NM_031221	0.02875	−0.26988	0.04810	−0.23432
204240_s_at	SMC2	NM_006444	0.03866	0.26490	0.01942	0.58069
218066_at	SLC12A7	NM_006598	0.00380	−0.25309	0.02545	−0.34822
204093_at	CCNH	NM_001239	0.04501	0.24875	0.02513	0.36585
203259_s_at	HDDC2	BC001671	0.03565	0.24591	0.04216	0.25357
203211_s_at	MTMR2	NM_016156	0.01090	0.23756	0.04171	0.35163
217168_s_at	HERPUD1	AF217990	0.02742	−0.23102	0.04095	−0.27275
212400_at	FAM102A	AL043266	0.02161	−0.23002	0.03518	−0.26290
219003_s_at	MANEA	AI587307	0.02986	0.22902	0.04405	0.61804
202558_s_at	STCH	NM_006948	0.00297	0.22535	0.01722	0.55860
201873_s_at	ABCE1	NM_002940	0.00231	0.21508	0.02729	0.38377
201338_x_at	GTF3A	NM_002097	0.01293	0.21389	0.02921	0.33993
222018_at	NACA	AI992187	0.02157	−0.21387	0.02880	−0.42430
201724_s_at	GALNT1	NM_020474	0.04119	0.20913	0.02122	0.33088
203202_at	KRR1	AI950314	0.00770	0.20388	0.02047	0.43561
210495_x_at	FN1	AF130095	0.04842	−0.19985	0.01893	−0.45837
202078_at	COPS3	NM_003653	0.03733	0.19943	0.02282	0.36856
1007_s_at	DDR1	U48705	0.01974	−0.19430	0.02195	−0.28211
205329_s_at	SNX4	AF130078	0.02782	0.19149	0.04777	0.38678
218535_s_at	RIOK2	NM_018343	0.01864	0.18852	0.03445	0.38006
213528_at	C1orf156	AL035369	0.03062	0.18361	0.04519	0.39024
217898_at	C15orf24	NM_020154	0.03086	0.18348	0.03855	0.30539
203633_at	CPT1A	BF001714	0.03196	−0.18225	0.03540	−0.42819
202541_at	SCYE1	BF589679	0.00457	0.18152	0.02629	0.33184
208838_at	CAND1	AB020636	0.02098	0.17682	0.02385	0.38415
214499_s_at	BCLAF1	AF249273	0.03844	0.17647	0.03006	0.45884
201144_s_at	EIF2S1	NM_004094	0.02885	0.17371	0.03789	0.29423
203016_s_at	SSX2IP	NM_014021	0.02366	0.17157	0.04422	0.44294
221525_at	ZMIZ2	AL136572	0.02424	−0.17123	0.02324	−0.28681
221652_s_at	C12orf11	AF274950	0.02948	0.17022	0.01925	0.41622
202906_s_at	NBN	AF049895	0.01848	0.15999	0.02014	0.36253
203831_at	R3HDM2	NM_014925	0.02060	−0.15758	0.03331	−0.38288
204906_at	RPS6KA2	BC002363	0.02098	−0.15753	0.03740	−0.24637
203565_s_at	MNAT1	NM_002431	0.00792	0.15731	0.04162	0.22754

TABLE III. (*Continued*)

			In vivo		In vitro	
Affymetrix probeset ID	Gene symbol	GenBank ID	*P*-value	Fold-change log 2 difference	*P*-value	Fold-change log 2 difference
218462_at	BXDC5	NM_025065	0.00337	0.15418	0.04931	0.27509
41386_i_at	JMJD3	AB002344	0.00984	−0.14874	0.00110	−0.74878
60528_at	LOC100137047-PLA2G4B	N71116	0.00701	−0.14740	0.03590	−0.22309
212070_at	GPR56	AL554008	0.04160	−0.14620	0.01131	−0.44151
203221_at	TLE1	NM_005077	0.01203	−0.14507	0.01724	−0.33364
221547_at	PRPF18	BC000794	0.01390	0.14082	0.03291	0.33321
212518_at	PIP5K1C	AB011161	0.04690	−0.14030	0.02796	−0.39628
202000_at	NDUFA6	BC002772	0.04603	0.13975	0.04390	0.22682
209313_at	XAB1	AB044661	0.00785	0.13961	0.04427	0.20051
203771_s_at	BLVRA	AA740186	0.03148	0.13743	0.03266	0.29603
218042_at	COPS4	NM_016129	0.01552	0.13598	0.02302	0.33442
202810_at	DRG1	NM_004147	0.02726	0.13521	0.04029	0.25094
218175_at	CCDC92	NM_025140	0.02888	−0.13469	0.01890	−0.35053
212794_s_at	KIAA1033	AK001728	0.01397	0.13410	0.04814	0.30668
40093_at	BCAM	X83425	0.04031	−0.13316	0.02780	−0.29525
203436_at	RPP30	NM_006413	0.00637	0.13200	0.04226	0.23522
214273_x_at	C16orf35	AV704353	0.03624	−0.13197	0.03587	−0.26605
202542_s_at	SCYE1	NM_004757	0.03275	0.12908	0.03818	0.26723
203293_s_at	LMAN1	NM_005570	0.01432	0.12722	0.04875	0.51005
214246_x_at	MINK1	AI859060	0.04187	−0.12251	0.00853	−0.43881
208642_s_at	XRCC5	AA205834	0.02250	0.12216	0.03838	0.32159
217829_s_at	USP39	NM_006590	0.03523	0.12029	0.04516	0.21099
207614_s_at	CUL1	NM_003592	0.02911	0.11716	0.04785	0.19762
202919_at	MOBKL3	NM_015387	0.04545	0.11694	0.02710	0.32444
218250_s_at	CNOT7	NM_013354	0.04001	0.11421	0.03772	0.31048
203033_x_at	FH	NM_000143	0.03778	0.11414	0.04239	0.23218
218203_at	ALG5	NM_013338	0.03227	0.11324	0.03358	0.18591
201857_at	ZFR	NM_016107	0.02351	0.11160	0.04035	0.28530
203712_at	KIAA0020	NM_014878	0.02615	0.11029	0.04537	0.17392
200079_s_at	KARS	AF285758	0.03959	0.10386	0.03727	0.35252
202511_s_at	ATG5	AK001899	0.02049	0.10342	0.03339	0.32196
205717_x_at	PCDHGC3	NM_002588	0.00222	−0.10159	0.04045	−0.43825
41660_at	CELSR1	AL031588	0.04452	−0.10142	0.03802	−0.23308
202512_s_at	ATG5	AK001899	0.04960	0.09543	0.03662	0.35297
205957_at	PLXNB3	NM_005393	0.01133	−0.07343	0.03702	−0.24197
215706_x_at	ZYX	BC002323	0.03440	−0.07226	0.01121	−0.36667
214585_s_at	VPS52	AL390171	0.01798	−0.05387	0.03360	−0.17258
218323_at	RHOT1	NM_018307	0.01979	0.04444	0.03443	0.25485
206862_at	ZNF254	NM_004876	0.00243	0.03647	0.02496	0.41548

Positive values indicate placebo expression was higher.
Affymetrix HG-U133Av2 microarray: comparison of gene expression changes in LuCaP 35 xenografts and LNCaP cells with dutasteride treatment.

changes in prostate cancer cells derived from two distinct sources, both of which can progress to androgen-deprivation independent growth over time following androgen ablation. Heterogeneous LuCaP 35 xenografts expressing wild-type AR and clonal LNCaP in vitro cells with a mutation in the AR ligand binding domain both respond to dutasteride treatment by activating genes in some common pathways. Delineating which pathways are critical for survival in prostate cells undergoing androgen deprivation will be an important outgrowth of this study.

DISCUSSION

Dutasteride is highly effective at lowering DHT levels in men with both BPH and prostate cancer, and is

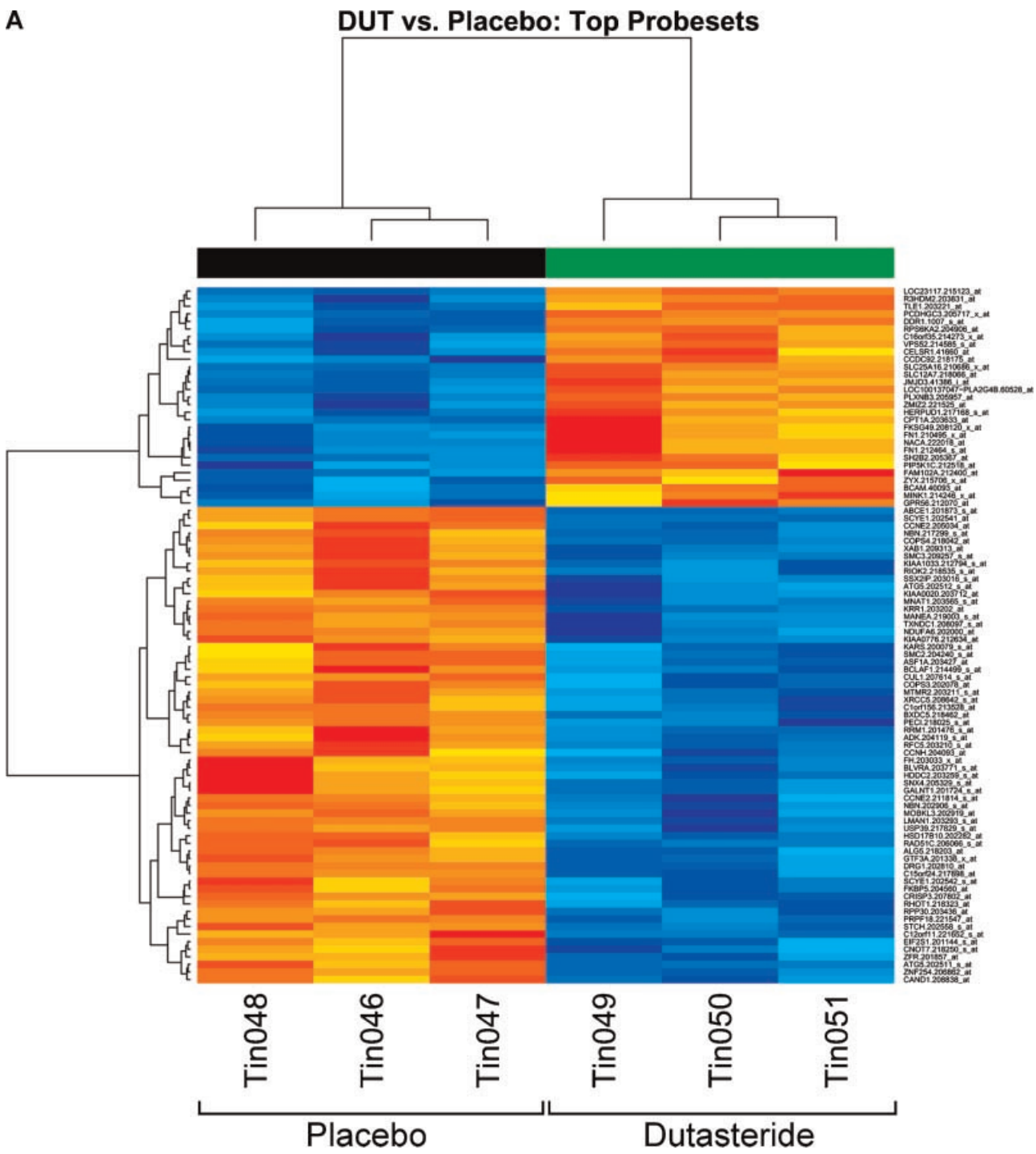

Fig. 6. **A**: Heatmap of the 92 common genes with *P*-values $\leq$0.05 affected by dutasteride treatment of prostate cancer cells, in vivo LuCaP 35 versus in vitro LNCaP, determined by microarray analysis. A comparison was run between results of Affymetrix HG-UI33Av2 arrays probed with three placebo- versus three dutasteride-treated xenografts and arrays probed with three vehicle- versus three dutasteride-treated cultures of LNCaP cells. Tin046 - 048 represent placebo/vehicle-treated samples with Tin049 - 051 representing dutasteride-treated samples. **B**: Pathway analysis was performed using MetaCore software, as described in Materials and Methods Section. Top 33 pathways containing genes significantly affected in LuCaP 35 xenografts with dutasteride treatment are shown as a bar graph indicating significance after adjusting for a false discovery rate of $P < 0.25$. Orange bars represent pathways with genes from LuCaP 35 data; blue bars indicate where common genes from comparison of LuCaP and LNCaP data fit into significant pathways.

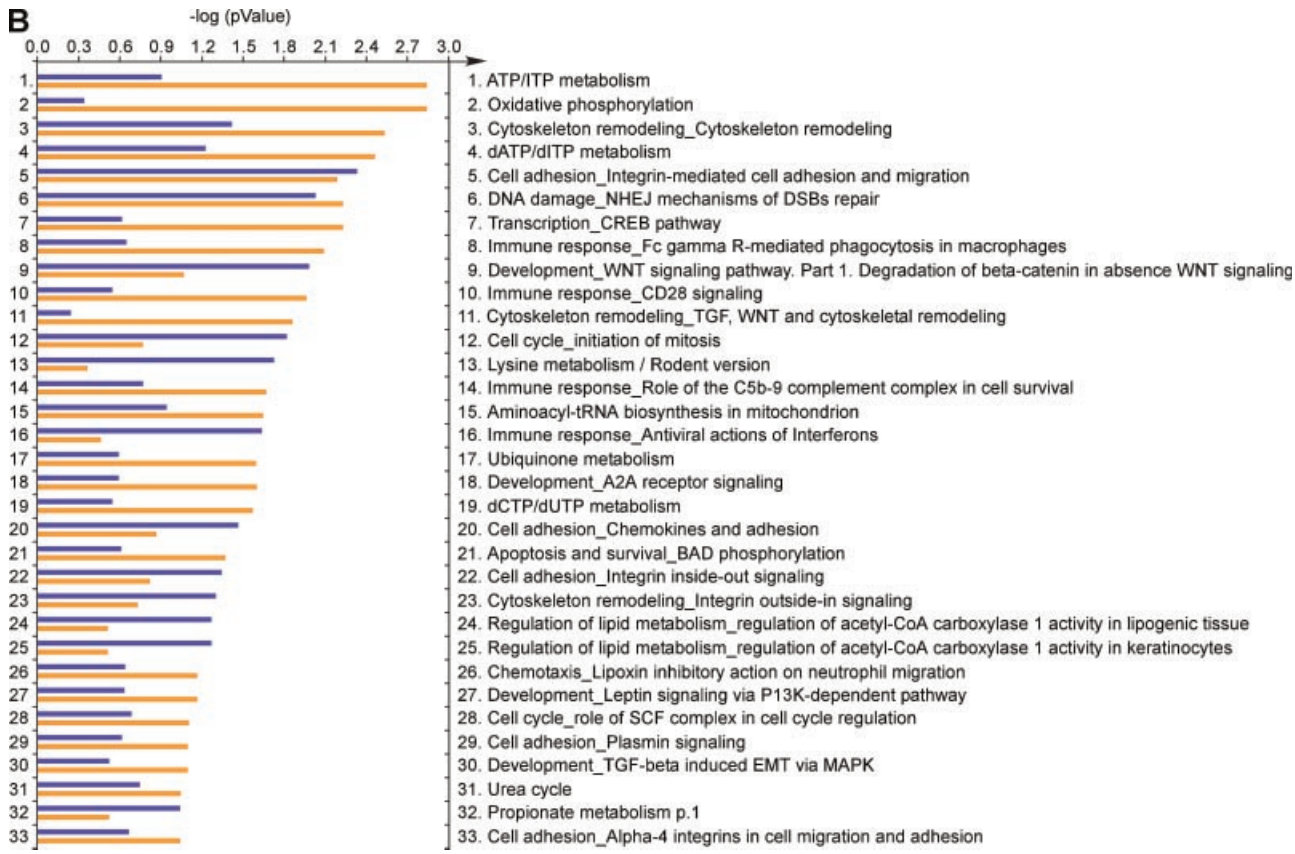

Fig. 6. (*Continued*)

currently being evaluated for its efficacy in reducing both the risk of developing prostate cancer in the REDUCE trial [1] and in treating prostate cancer in the REDEEM trial [2]. In view of this, it is important to understand how dutasteride is working in prostate cancer cells at the molecular level and what changes are occurring in these cells in response to the drastic reduction in DHT achieved by treatment. Our previous work with prostate cancer cell lines in vitro identified genes and pathways involved in cell cycle regulation, apoptosis, and fatty acid metabolism, in addition to the androgenic pathway, as being affected by dutasteride treatment. In the current study we extended these findings into a mouse xenograft model and discovered new pathways, such as Rho GTPase regulation of cytoskeleton remodeling, which helped to elucidate how prostate cells are responding to this drug in the context of the tumor microenvironment.

It has been demonstrated previously by molecular profiling of a related xenograft LuCaP 23.1, that different populations of cells exist in these tumors which exhibit distinct molecular profiles as they progress to androgen independence following androgen ablation [20]. Similarly, the LuCaP 35 xenografts we have used in this study exhibited different rates of growth, with some tumors growing much more rapidly than others. We initially sorted our mice into matched pairs based on initial tumor volumes and included tumors with varying growth rates in our study groups. We have demonstrated that though these tumors grow at different rates, dutasteride significantly decreased the growth rate in all of the treated tumors and can exert similar effects on heterogeneous cell populations through some common pathways, regardless of the tumor's initial molecular profile.

CONCLUSION

Reduction of DHT by inhibition of 5AR activity is a legitimate approach in the attempt to reduce the risk of prostate cancer development and also is a potentially valuable tool in disease management. However, it is known that androgen-deprivation therapy does not completely inactivate the androgen axis and that prostate tumor cells eventually progress to a castration-recurrent state. By defining how an SRD5I like dutasteride is working at the molecular level in prostate tumors it may be possible to develop better agents that can be used in combination with this drug to further enhance its effectiveness.

ACKNOWLEDGMENTS

We thank GlaxoSmithKline for providing us with dutasteride, Dr. Robert Vessella at the University of Washington School of Medicine, Seattle, Washington for the implantable LuCaP 35 xenograft tissue, the Mayo Advanced Genomic Technology Center Microarray Shared Resource for array processing, and Ken Peters for his help with manuscript preparation. Funding for this study was provided by NCI Grant numbers: CA121277, CA125747, CA91956, a grant from the T.J. Martell Foundation and Grant number 144 from GlaxoSmithKline.

REFERENCES

1. Andriole G, Bostwick D, Brawley O, Gomella L, Marberger M, Tindall D, Breed S, Somerville M, Rittmaster R. Chemoprevention of prostate cancer in men at high risk: Rationale and design of the reduction by dutasteride of prostate cancer events (REDUCE) trial. J Urol 2004;172(4 Pt 1):1314–1317.
2. Fleshner N, Gomella LG, Cookson MS, Finelli A, Evans A, Taneja SS, Lucia MS, Wolford E, Somerville MC, Rittmaster R. Delay in the progression of low-risk prostate cancer: Rationale and design of the Reduction by Dutasteride of Clinical Progression Events in Expectant Management (REDEEM) trial. Contemp Clin Trials 2007;28(6):763–769.
3. Lazier CB, Thomas LN, Douglas RC, Vessey JP, Rittmaster RS. Dutasteride, the dual 5alpha-reductase inhibitor, inhibits androgen action and promotes cell death in the LNCaP prostate cancer cell line. Prostate 2004;58(2):130–144.
4. Schmidt LJ, Murillo H, Tindall DJ. Gene expression in prostate cancer cells treated with the dual 5 alpha-reductase inhibitor dutasteride. J Androl 2004;25(6):944–953.
5. Shao TC, Li H, Ittmann M, Cunningham GR. Effects of dutasteride on prostate growth in the large probasin-large T antigen mouse model of prostate cancer. J Urol 2007;178(4 Pt 1):1521–1527.
6. Xu Y, Dalrymple SL, Becker RE, Denmeade SR, Isaacs JT. Pharmacologic basis for the enhanced efficacy of dutasteride against prostatic cancers. Clin Cancer Res 2006;12(13):4072–4079.
7. Schmidt LJ, Ballman KV, Tindall DJ. Inhibition of fatty acid synthase activity in prostate cancer cells by dutasteride. Prostate 2007;67(10):1111–1120.
8. Ballman KV, Grill DE, Oberg AL, Therneau TM. Faster cyclic loess: Normalizing RNA arrays via linear models. Bioinformatics 2004;20(16):2778–2786.
9. Dudoit S, Yang YH, Callow MJ, Speed TP. Statistical methods for identifying differentially expressed genes in replicated cDNA microarray experiments. Stat Sinica 2002;12(1):111–139.
10. Irizarry RA, Hobbs B, Collin F, Beazer-Barclay YD, Antonellis KJ, Scherf U, Speed TP. Exploration, normalization, and summaries of high density oligonucleotide array probe level data. Biostatistics 2003;4(2):249–264.
11. Benjamini YaH Y. Controlling the false discovery rate: A practical and powerful approach to multiple testing. J R Stat Soc 1995;B(58):289–300.
12. Corey E, Quinn JE, Buhler KR, Nelson PS, Macoska JA, True LD, Vessella RL. LuCaP 35: A new model of prostate cancer progression to androgen independence. Prostate 2003;55(4):239–246.
13. Bjartell AS, Al-Ahmadie H, Serio AM, Eastham JA, Eggener SE, Fine SW, Udby L, Gerald WL, Vickers AJ, Lilja H, Reuter VE, Scardino PT. Association of cysteine-rich secretory protein 3 and beta-microseminoprotein with outcome after radical prostatectomy. Clin Cancer Res 2007;13(14):4130–4138.
14. Biancolella M, Valentini A, Minella D, Vecchione L, D'Amico F, Chillemi G, Gravina P, Bueno S, Prosperini G, Desideri A, Federici G, Bernardini S, Novelli G. Effects of dutasteride on the expression of genes related to androgen metabolism and related pathway in human prostate cancer cell lines. Invest New Drugs 2007;25(5):491–497.
15. Heemers HV, Regan KM, Schmidt LJ, Anderson SK, Ballman KV, Tindall DJ. Androgen modulation of coregulator expression in prostate cancer cells. Mol Endocrinol 2009;23(4):572–583.
16. Lyons LS, Rao S, Balkan W, Faysal J, Maiorino CA, Burnstein KL. Ligand-independent activation of androgen receptors by Rho GTPase signaling in prostate cancer. Mol Endocrinol 2008;22(3):597–608.
17. Lyons LS, Burnstein KL. Vav3, a Rho GTPase guanine nucleotide exchange factor, increases during progression to androgen independence in prostate cancer cells and potentiates androgen receptor transcriptional activity. Mol Endocrinol 2006;20(5):1061–1072.
18. Tam SW, Theodoras AM, Pagano M. Kip1 degradation via the ubiquitin-proteasome pathway. Leukemia 1997;11(Suppl 3):363–366.
19. Yang G, Ayala G, De Marzo A, Tian W, Frolov A, Wheeler TM, Thompson TC, Harper JW. Elevated Skp2 protein expression in human prostate cancer: Association with loss of the cyclin-dependent kinase inhibitor p27 and PTEN and with reduced recurrence-free survival. Clin Cancer Res 2002;8(11):3419–3426.
20. Fina F, Muracciole X, Rocchi P, Nanni-Metellus I, Delfino C, Daniel L, Dussert C, Ouafik L, Martin PM. Molecular profile of androgen-independent prostate cancer xenograft LuCaP 23.1. J Steroid Biochem Mol Biol 2005;96(5):355–365.